Casimir energies and general relativity energy conditions

2006 J. Phys. A: Math. Gen. 39 6423

(http://iopscience.iop.org/0305-4470/39/21/S37)

INSTITUTE OF PHYSICS PUBLISHING JOURNAL OF PHYSICS A: MATHEMATICAL AND GENERAL

J. Phys. A: Math. Gen. **39** (2006) 6423–6431 doi:10.1088/0305-4470/39/21/S37

Casimir energies and general relativity energy conditions

Noah Graham

Department of Physics, Middlebury College Middlebury, VT 05753, USA

E-mail: ngraham@middlebury.edu

Received 7 November 2005, in final form 4 January 2006
Published 10 May 2006
Online at stacks.iop.org/JPhysA/39/6423

Abstract

Quantum systems often contain negative energy densities. In general relativity, negative energies lead to time advancement, rather than the usual time delay. As a result, some Casimir systems appear to violate energy conditions that would protect against exotic phenomena such as closed timelike curves and superluminal travel. However, when one examines a variety of Casimir systems using self-consistent approximations in quantum field theory, one finds that a particular energy condition is still obeyed, which rules out exotic phenomena. I will discuss the methods and results of these calculations in detail and speculate on their potential implications in general relativity.

PACS numbers: 03.65.Nk, 04.20.Gz

(Some figures in this article are in colour only in the electronic version)

1. Introduction

General relativity allows spacetimes of any geometry. Given any $g_{\mu\nu}$, we can compute $R_{\mu\nu}$ and R, and then set up a matter configuration whose stress–energy tensor is

$$T_{\mu\nu} = \frac{1}{8\pi G}\left(R_{\mu\nu} - \frac{1}{2}g_{\mu\nu}R\right) \tag{1}$$

to obtain a solution to Einstein's equations with the desired geometry. As a result, nothing seems to prohibit the existence of exotic phenomena such as closed timelike curves [1], traversable wormholes [2] or superluminal travel [3]. Therefore, we expect there to exist some restrictions on the possible tensors $T_{\mu\nu}$, usually called energy conditions, which would lead to restrictions on the possible spacetime geometries. While it is straightforward to show that classical field theories obey energy conditions that are strong enough to forbid exotic phenomena, quantum field theories appear to violate these conditions.

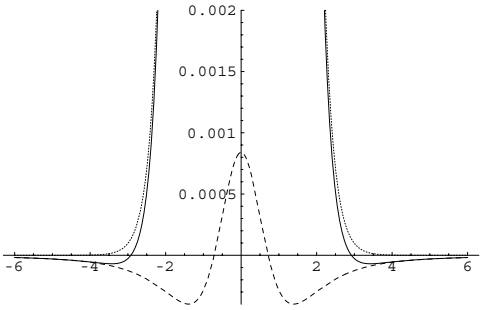

Figure 1. Classical energy density due to the wall (dotted), the quantum correction (dashed) and the total (solid) for typical values of the coupling constants.

We will focus on the following energy conditions.

- The weak energy condition (WEC) requires that for all timelike vectors V^μ,

$$T_{\mu\nu}V^\mu V^\nu \geqslant 0. \tag{2}$$

  That is, all observers see positive energy density.
- The null energy condition (NEC) is weaker than the WEC, and requires that equation (2) hold only for null vectors V^μ.
- The averaged null energy condition (ANEC) is weaker than the NEC, and only requires that the NEC hold when integrated over a complete null geodesic.

In a classical background, all of these conditions can be imposed consistently, and any one of them would be sufficient to rule out exotic phenomena [1]. On the other hand, the standard Casimir system of parallel conducting plates has a static negative energy between the plates, and thus it appears to violate all of these conditions. However, there are some obvious caveats to this result. An external agent has to hold the plates apart, and impose the boundary condition. Furthermore, in the case of ANEC, the geodesic has to go through the boundary, where we are ignoring the effects of the material. Since gravity couples to all sources of stress–energy, we cannot consider the contribution of the Casimir energy without also including the contributions due to the materials and their internal interactions.

Previous work [4, 5] avoided these problems by considering a domain wall background that is renormalized with standard counterterms. In this way, all the contributions to the stress–energy tensor can be included. The result, shown in figure 1, is that for any coupling, there is always a small region at large enough x, where the energy density is negative. So we can always choose the coupling small enough that our semiclassical approximation is reliable and still find negative energies. This situation also violates quantum inequalities [6–8]. Although this system violates WEC, since we have a region of negative energy density, and NEC, if we take a null vector in the region of negative energy pointing perpendicular to the wall, ANEC is still obeyed, since the contribution from the complete geodesic perpendicular to the wall is only negative if the total energy of the domain wall is negative (indicating an unstable vacuum and a breakdown of our approximation).

In a number of other examples, explicit calculation shows that ANEC is obeyed. These include a geodesic outside a spherically symmetric background potential [9] or a dielectric sphere [10]. Other calculations also show that energy condition violation is more difficult to achieve in realistic situations than idealized models would suggest [11, 12]. ANEC is also known to be obeyed by free scalar [13] and electromagnetic [14] fields in flat spacetime. Other works have found restrictions on energy condition violation in flat space [6, 15, 16].

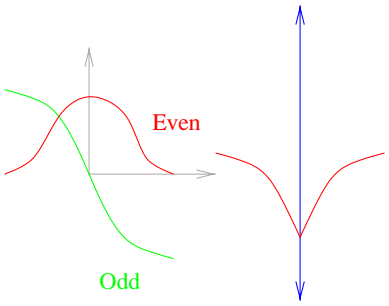

Figure 2. In free space (left) we have even and odd normal mode wavefunctions. In the presence of a Dirichlet plate (right), the even functions are replaced by the odd functions with a change of sign crossing the plate.

2. Plate with a hole calculation

To further investigate ANEC, work done in collaboration with Olum [17] considers another alternative. We avoid the plate by drilling a hole in it for the geodesic to travel through. Then we might expect that the region around the hole would provide only a small correction to the negative contribution from the rest of the geodesic, yielding a violation of ANEC. Since the geodesic never encounters the material, the result will be finite with no contributions from the counterterms (which have support only where there is a potential). Our approach will be to use a Babinet's principle argument to show that the Casimir energy of a Dirichlet plate with a hole is the sum of the Casimir energy of a full Dirichlet plate and the Casimir energy of a Neumann disc. Then we will use scattering theory in ellipsoidal coordinates to solve the disc problem, and add in the standard result for the full plate.

In free space, we can decompose the spectrum into modes that are odd or even under reflection of the z-axis. Imposing a Dirichlet boundary condition at $z = 0$ has no effect on the odd modes, since they already obey the boundary condition. However, the even modes are modified; they turn into the odd modes multiplied by the sign of z, with a cusp at $z = 0$, as shown in figure 2.

If there is a hole in the plate, we find even functions that obey Neumann conditions in the hole (since they are even) and Dirichlet conditions elsewhere. Up to a similar sign flip between positive and negative z, these are the same functions as one obtains for the odd modes of a Neumann patch with the same shape as the hole, as shown in figure 3.

Let E be the contribution to the Casimir energy from the free even modes, O be the contribution to the Casimir energy from the free odd modes and A be the contribution to the Casimir energy from the modes for the plate with the hole. Then we have the following total contributions to the energy, where we have taken the difference with the free space result:

$$\begin{aligned}
&\text{free space:} && E + O && \xrightarrow{\text{subtract free space}} && \text{zero}\\
&\text{Dirichlet plate:} && O + O && \xrightarrow{\text{subtract free space}} && O - E\\
&\text{Dirichlet plate with hole:} && A + O && \xrightarrow{\text{subtract free space}} && A - E\\
&\text{Neumann disc:} && E + A && \xrightarrow{\text{subtract free space}} && A - O.
\end{aligned}$$

Thus we have found

$$[\text{Dirichlet plate with a hole}] = [\text{Neumann disc}] + [\text{Dirichlet plate}]. \tag{3}$$

Next, we set up the disc problem. We will begin in two space dimensions and find the Casimir energy of a Neumann line segment. For notational consistency with the

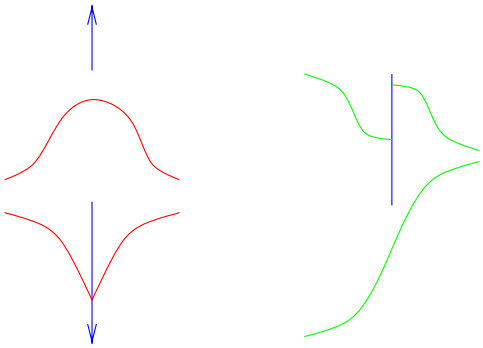

Figure 3. If there is a hole in the Dirichlet plate (left), the new even functions satisfy Neumann conditions in the hole and Dirichlet conditions elsewhere. The odd functions for a Neumann patch with the same shape as the hole (right) are the same except for a change of sign between sides.

three-dimensional case, we consider the x–z plane with the geodesic running along the z-axis and the segment running along the x-axis from $x = -d$ to $x = d$. We define elliptical coordinates μ and θ by

$$x = d\cosh\mu\cos\theta \qquad z = d\sinh\mu\sin\theta \tag{4}$$

and then the boundary condition is applied at the points where the radial coordinate μ is zero. In elliptical coordinates, the problem is still separable, but there is no analogue of angular momentum conservation. We still have separate angular and radial functions, but we now have the additional dimensionful parameter d. Thus the angular functions are now not simply functions of θ; they can now depend also on kd, where k is the wave number. Similarly the radial functions can depend on kd and r/d separately, rather than depending simply on the product kr.

As described above, we have normal mode solutions that are even and odd under reflection of the z-axis. Since the line segment has Neumann boundary conditions, only the odd modes need to be modified from the free case. These become

$$\psi o_m(\mu, q) = \tfrac{1}{2}\left[\mathrm{e}^{2\mathrm{i}\delta} Ho_m^{(1)}(\mu, q) + Ho_m^{(2)}(\mu, q)\right] se_m(\theta, q) \tag{5}$$

where $q = (\mathrm{d}k/2)^2$. Here $se_m(\theta, q)$ is the odd angular Mathieu function and $Ho_m^{(1)}$ and $Ho_m^{(2)}$ are the corresponding odd radial functions of the third and fourth kinds, with $Ho_m^{(1)} = Jo_m + \mathrm{i}Yo_m$ and $Ho_m^{(2)} = Jo_m - \mathrm{i}Yo_m$, where Jo_m and Yo_m are the radial functions of the first and second kind respectively. The phase shift $\delta(q)$ is defined by imposing the boundary condition, which yields

$$\mathrm{e}^{2\mathrm{i}\delta} = -\frac{Ho_m^{(2)\prime}(0, q)}{Ho_m^{(1)\prime}(0, q)} \tag{6}$$

where the derivative is with respect to μ.

We have adopted the normalization conventions of [18], but have modified their notation to make the analogy to the circular case clearer. In these conventions, the even and odd angular functions $ce_m(\theta, q)$ and $se_m(\theta, q)$ are normalized just like the $\cos m\theta$ and $\sin m\theta$ solutions in the circular case, so that

$$\int_0^{2\pi} \mathrm{d}\theta\, ce_m(\theta, q)^2 = \int_0^{2\pi} \mathrm{d}\theta\, se_m(\theta, q)^2 = \pi. \tag{7}$$

As in the circular case, $m = 0, 1, 2, 3\ldots$ for the even functions[1] and $m = 1, 2, 3\ldots$ for the odd functions. The radial functions are then normalized so that they approach the corresponding Bessel functions at large radius[2]. Instead of singularities at zero radius as in the circular case, the radial functions of the second kind have jump discontinuities—the singularity is now 'spread' over the interfocal separation.

From these wavefunctions, we form the normalized quantum field ϕ:

$$\phi(\mu,\theta) = \sum_{m=0}^{\infty}\int_0^{\infty} \mathrm{d}k\sqrt{\frac{k}{2\pi\omega}}\left(Je_m(\mu,q)ce_m(\theta,q)\hat{b}_k^{m\dagger} + Jo_m(\mu,q)se_m(\theta,q)\hat{c}_k^{m\dagger}\right)\mathrm{e}^{\mathrm{i}\omega t} + \text{complex conjugate}, \tag{8}$$

where the odd term vanishes for $m = 0$. The stress–energy tensor for a minimally-coupled scalar field is

$$T_{\lambda\nu} = \partial_\lambda\phi\partial_\nu\phi - \tfrac{1}{2}\eta_{\lambda\nu}[\partial^\lambda\phi\partial_\lambda\phi]. \tag{9}$$

For a null vector, $\eta_{\lambda\nu}V^\lambda V^\nu = 0$, so we have

$$T_{\lambda\nu}V^\lambda V^\nu = (V^\alpha\partial_\alpha\phi)^2\,. \tag{10}$$

Taking our geodesic along the z-axis, $V = (1, \hat{\mathbf{z}})$, we have

$$T_{\lambda\nu}V^\lambda V^\nu = \dot{\phi}^2 + (\partial_z\phi)^2\,. \tag{11}$$

We then substitute the result for the quantum field into this expression, subtract the free space result and take the vacuum expectation value [9, 20–22]. For computational efficiency, we extend the k integration to the whole real axis and use contour integration to obtain an integral over the imaginary k-axis, using $k = \mathrm{i}\kappa$. We obtain [17]

$$\langle\dot{\phi}^2\rangle = \frac{1}{\pi^2}\sum_{m=1}^{\infty}\int_0^{\infty}\mathrm{d}\kappa\,\frac{Io_m'(0,\varphi)}{Ko_m'(0,\varphi)}\kappa^2 Ko_m(\mu,\varphi)^2 se_m(\theta,-\varphi)^2. \tag{12}$$

On the z-axis, terms with m even vanish, so we have

$$\langle\dot{\phi}^2\rangle = \frac{1}{\pi^2}{\sum_{m=1}^{\infty}}'\int_0^{\infty}\mathrm{d}\kappa\,\frac{Io_m'(0,\varphi)}{Ko_m'(0,\varphi)}\kappa^2 Ko_m(\mu,\varphi)^2 se_m(\pi/2,-\varphi)^2, \tag{13}$$

where the prime on the summation sign indicates that we sum over odd values of m. The sum over channels and integral over k are absolutely convergent, since we have subtracted the contribution of the free theory and we are away from the interactions, where all the remaining counterterms vanish. Similarly, on the z-axis we have

$$\langle(\partial_z\phi)^2\rangle = -\frac{1}{\pi^2 d^2\cosh^2\mu}{\sum_{m=1}^{\infty}}'\int_0^{\infty}\mathrm{d}\kappa\,\frac{Io_m'(0,\varphi)}{Ko_m'(0,\varphi)}Ko_m'(\mu,\varphi)^2 se_m(\pi/2,-\varphi)^2. \tag{14}$$

In three dimensions, we employ oblate ellipsoidal coordinates,

$$x = d\sqrt{(\xi^2+1)(1-\eta^2)}\cos\phi \qquad y = d\sqrt{(\xi^2+1)(1-\eta^2)}\sin\phi \qquad z = d\eta\xi, \tag{15}$$

using the conventions of [23]. As in spherical coordinates, the solutions are indexed by $n = 0, 1, 2, 3\ldots$ and $m = -n, \ldots, n$. The angular solutions are spheroidal harmonics $\mathcal{Y}_n^m(\mathrm{i}c;\eta,\phi)$, where $c = kd, \cos^{-1}\eta$ is the polar angle and ϕ is the azimuthal angle. These are normalized analogously to ordinary spherical harmonics. The radial functions

[1] In the circular case, for $m = 0$ the even solution is a constant, which is normalized to be $\frac{1}{\sqrt{2}}$ rather than $\cos 0 = 1$, so that its normalization is consistent with the other modes.

[2] Note that the functions Je_m and Jo_m defined in [19] have an additional factor of $\sqrt{\pi/2}$.

are $R_n^{m(1)}(\mathrm{i}c;-\mathrm{i}\xi)$ and $R_n^{m(2)}(\mathrm{i}c;-\mathrm{i}\xi)$, where ξ is the radial coordinate. These are normalized so that they approach the usual spherical Bessel functions at large radius. The factors of $\pm\mathrm{i}$ convert from prolate to oblate coordinates.

Now we consider Neumann boundary conditions on the disc $\xi = 0$. If $m+n$ is even, the functions obey the boundary conditions already. Otherwise we need to take a combination of $R_n^{m(1)}$ and $R_n^{m(2)}$. With $R_n^{m(3)} = R_n^{m(1)} + \mathrm{i}R_n^{m(2)}$ and $R_n^{m(4)} = R_n^{m(1)} - \mathrm{i}R_n^{m(4)}$ we can write the desired radial function

$$\psi_n^m(\mathrm{i}c;-\mathrm{i}\xi) = \tfrac{1}{2}\left[\mathrm{e}^{2\mathrm{i}\delta(\mathrm{i}c)}R_n^{m(3)}(\mathrm{i}c;-\mathrm{i}\xi) + R_n^{m(4)}(\mathrm{i};-\mathrm{i}\xi)\right] \tag{16}$$

with the condition

$$\mathrm{e}^{2\mathrm{i}\delta(\mathrm{i})} = -\frac{R_n^{m(4)\prime}(\mathrm{i}c;0)}{R_n^{m(3)\prime}(\mathrm{i}c;0)} \tag{17}$$

where the derivative is with respect to the second argument.

Passing to the imaginary k-axis in the same way as in the two-dimensional case, we obtain [17]

$$\langle\dot\phi^2\rangle = -\frac{1}{\pi}\sum_{n=0}^{\infty}{\sum_{m=-n}^{n}}'\int_0^\infty \mathrm{d}\kappa\,\kappa^3\frac{R_n^{m(1)\prime}(\gamma;0)}{R_n^{m(3)\prime}(\gamma;0)}\left|\mathcal{Y}_n^m(\gamma;\eta,\phi)\right|^2 R_n^{m(3)}(\gamma;-\mathrm{i}\xi)^2, \tag{18}$$

where $\gamma = \mathrm{i}c = \mathrm{i}kd = -\kappa d$ and the prime on the summation sign means that only odd values of $m+n$ are included. On the axis, we have

$$\langle\dot\phi^2\rangle = -\frac{1}{\pi}{\sum_{n=1}^{\infty}}'\int_0^\infty \mathrm{d}\kappa\,\kappa^3\frac{R_n^{0(1)\prime}(\gamma;0)}{R_n^{0(3)\prime}(\gamma;0)}\left|\mathcal{Y}_n^0(\gamma;1,\phi)\right|^2 R_n^{0(3)}(\gamma;-\mathrm{i}\xi)^2, \tag{19}$$

where we have specialized to $m=0$ because the contributions from nonzero m vanish on the axis, leaving only a sum over odd values of n. Similarly, on the axis we have

$$\langle(\partial_z\phi)^2\rangle = -\frac{1}{\pi d^2}{\sum_{n=1}^{\infty}}'\int_0^\infty \mathrm{d}\kappa\,\kappa\frac{R_n^{0(1)\prime}(\gamma;0)}{R_n^{0(3)\prime}(\gamma;0)}\left|\mathcal{Y}_n^0(\gamma;1,\phi)\right|^2 R_n^{0(3)\prime}(\gamma;-\mathrm{i}\xi)^2 \tag{20}$$

where the primes on the radial functions indicate derivatives with respect to the second argument.

Once we have computed the result for a Neumann segment and disc, we must simply combine with the Dirichlet mirror result (see for example [24]),

$$\langle\dot\phi^2\rangle + \langle(\partial_z\phi)^2\rangle = \begin{cases} -\dfrac{1}{32\pi z^3} & \text{in two dimensions, and} \\ -\dfrac{1}{16\pi^2 z^4} & \text{in three dimensions.} \end{cases} \tag{21}$$

3. Results

We carried out the two-dimensional calculations using the C++ Mathieu function package of Alhargan [25, 26], with minor enhancements to accommodate the extreme range of Mathieu functions needed to accurately compute this sum. We have also adapted the code to use our normalization conventions instead of those of [19]. The sums and integrals are then done by calling the C++ code from Mathematica routines[3]. In three dimensions, we used the Mathematica spheroidal packages of Falloon [27], with minor enhancements to avoid memory

[3] Mathematica does provide built-in support for both radial and angular Mathieu functions, but only for functions of the first kind (as of version 5.2).

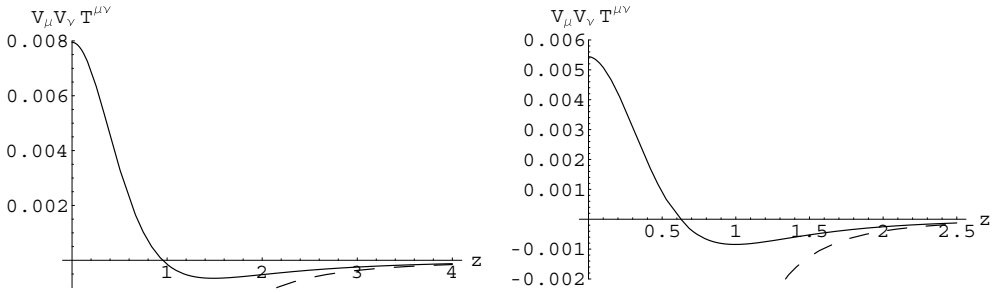

Figure 4. Contributions to NEC in two dimensions (left) and three dimensions (right) for a Dirichlet plate with a hole of unit radius, as functions of distance along the axis passing through the centre of the hole. Extrapolation is used for points at a distance less than 0.15 in the left panel and 0.25 in the right panel. The dotted lines show the perfect mirror result.

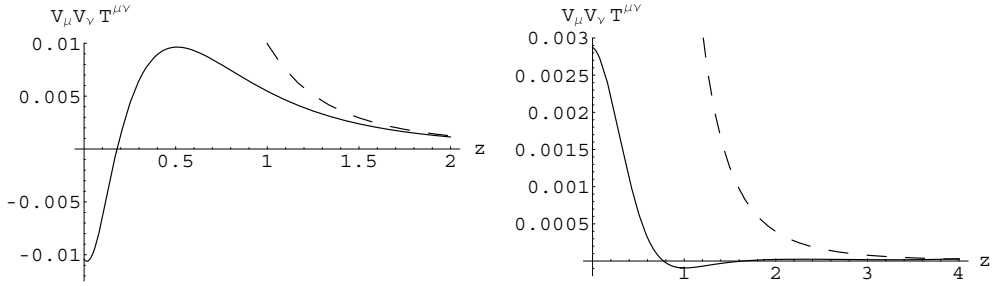

Figure 5. Contributions to NEC in two dimensions (left) and three dimensions (right) for a Neumann plate with a hole of unit radius, as functions of distance along the axis passing through the centre of the hole. Extrapolation is used for points at a distance less than 0.11 in the left panel and 0.25 in the right panel. The dotted lines show the perfect mirror result.

leaks, allow compatibility with current versions of Mathematica and improve efficiency for our application. Results in two and three dimensions are shown in figure 4. We see that in both cases the hole has a dramatic effect, overwhelming the NEC-violating behaviour away from the plate so that ANEC is obeyed. Although all field theory divergences are well under control, this calculation is still highly nontrivial for points near the hole, because both the perfect mirror and the disc have energies that diverge like $1/z^{n+1}$ where n is the space dimension and z is the distance to the hole. The final result, however, is perfectly finite—the origin is just a point in empty space. As a result, we have to stop our calculation a fixed distance away from the origin, depending on our numerical precision (and patience). We then extrapolate the result to zero, and verify that it goes to a finite result with zero slope (without building this requirement into the extrapolation). Far away, the calculation approaches the perfect mirror result, which is also shown in figure 4.

Since the Dirichlet plate with a hole obeys ANEC, and the Neumann and Dirichlet cases typically contribute with opposite signs, we might then expect a Neumann plate to violate ANEC, with a negative contribution from the hole overwhelming the positive contribution from far away. It is straightforward to repeat this analysis for that case [17]. However, as shown in figure 5, we see that ANEC is also obeyed for a Neumann plate with a hole. Furthermore, both the Dirichlet and Neumann results extend to the case of two plates in the limit of both large and small holes [17].

4. Conclusions

Energy condition violation by Casimir systems initially looks dramatic, but in consistent field theory models it is modest or nonexistent. We do not have an example of ANEC violation in flat space—that is, due to quantum effects in a background of non-gravitational quantum fields. Violations are known to exist [28–31] in curved space, when one considers the quantum effects of curvature caused by distant masses. But the magnitude of this violation is typically much smaller than competing effects associated with the source of the curvature itself (unless we consider Planck-scale objects, where classical general relativity is unreliable), so it is not clear that this violation will persist in the full theory. If ANEC (possibly with appropriate modifications in curved space) is always obeyed by realistic quantum field theories with no uncontrolled external agents, it would prevent the appearance of exotic phenomena. Work is underway to investigate the possibility of finding analytic arguments to ensure that ANEC is always obeyed in flat space.

Acknowledgments

This work was done in collaboration with Ken Olum (Tufts). NG was supported in part by a Cottrell College Science Award from Research Corporation and by a Baccalaureate College Development grant from the Vermont Experimental Program to Stimulate Competitive Research (VT-EPSCoR).

References

[1] Hawking S W 1992 Chronology protection conjecture *Phys. Rev.* D **46** 603–11
[2] Morris M S, Thorne K S and Yurtsever U 1988 Wormholes, time machines, and the weak energy condition *Phys. Rev. Lett.* **61** 1446
[3] Olum K D 1998 Superluminal travel requires negative energies *Phys. Rev. Lett.* **81** 3567–70
[4] Graham N and Olum K D 2003 Negative energy densities in quantum field theory with a background potential *Phys. Rev.* D **67** 085014
[5] Olum K D and Graham N 2003 Static negative energies near a domain wall *Phys. Lett.* B **554** 175–9
[6] Ford L H and Roman T A 1995 Averaged energy conditions and quantum inequalities *Phys. Rev.* D **51** 4277 (*Preprint* gr-qc/9410043)
[7] Ford L H and Roman T A 1997 Restrictions on negative energy density in flat spacetime *Phys. Rev.* D **55** 2082 (*Preprint* gr-qc/9607003)
[8] Pfenning M J and Ford L H 1998 Scalar field quantum inequalities in static spacetimes *Phys. Rev.* D **57** 3489 (*Preprint* gr-qc/9710055)
[9] Schwartz-Perlov D and Olum K D 2003 Null energy conditions outside a background potential *Phys. Rev.* D **68** 065016
[10] Graham N, Olum K D and Schwartz-Perlov D 2004 Energy conditions outside a dielectric ball *Phys. Rev.* D **70** 105019
[11] Sopova V and Ford L H 2002 The energy density in the Casimir effect *Phys. Rev.* D **66** 045026
[12] Sopova V and Ford L H 2005 The electromagnetic field stress tensor between dielectric half-spaces *Phys. Rev.* D **72** 033001
[13] Klinkhammer G 1991 Averaged energy conditions for free scalar fields in flat spacetime *Phys. Rev.* D **43** 2542
[14] Folacci A 1992 Averaged null energy condition for electromagnetism in Minkowski space-time *Phys. Rev.* D **46** 2726–9
[15] Borde A, Ford L H and Roman T A 2002 Constraints on spatial distributions of negative energy *Phys. Rev.* D **65** 084002
[16] Ford L H and Roman T A 1996 Averaged energy conditions and evaporating black holes *Phys. Rev.* D **53** 1988
[17] Graham N and Olum K D 2005 Plate with a hole obeys the averaged null energy condition *Phys. Rev.* D **72** 025013
[18] Abramowitz M and Stegun I A 1972 *Handbook of Mathematical Functions With Formulas, Graphs, and Mathematical Tables* (Washington: US Government Printing Office)

[19] McCord Morse P and Feshbach H 1953 *Methods of Theoretical Physics* (New York: McGraw-Hill)
[20] Bordag M and Lindig J 1996 Vacuum energy density in arbitrary background fields *J. Phys. A: Math. Gen.* **29** 4481–92
[21] Saharian A A 2001 Scalar Casimir effect for d-dimensional spherically symmetric robin boundaries *Phys. Rev.* D **63** 125007
[22] Graham N, Jaffe R L, Khemani V, Quandt M, Scandurra M and Weigel H 2002 Calculating vacuum energies in renormalizable quantum field theories: a new approach to the Casimir problem *Nucl. Phys.* B **645** 49–84
[23] Meixner J W and Schäfke R W 1954 *Mathieusche Funktionen und Sphäroidfunktionen* (Berlin: Springer)
[24] Mostepanenko V M and Trunov N N 1997 *The Casimir Effect and its Applications* (Oxford: Clarendon)
[25] Alhargan F 2000 Algorithms for the computation of all Mathieu functions of integer orders *ACM Trans. Math. Softw.* **26** 390–407
[26] Alhargan F 2000 Algorithm 804: subroutines for the computation of Mathieu functions of integer orders *ACM Trans. Math. Softw.* **26** 408–14
[27] Falloon P E, Abbott P C and Wang J B 2003 Theory and computation of the spheroidal wavefunctions *J. Phys. A: Math. Gen.* **36** 5477–95
[28] Visser M 1996 Gravitational vacuum polarization: I. Energy conditions in the Hartle-Hawking vacuum *Phys. Rev.* D **54** 5103 (*Preprint* gr-qc/9604007)
[29] Visser M 1996 Gravitational vacuum polarization: II. Energy conditions in the Boulware vacuum *Phys. Rev.* D **54** 5116 (*Preprint* gr-qc/9604008)
[30] Visser M 1996 Gravitational vacuum polarization: III. Energy conditions in the (1+1)-dimensional Schwarzschild spacetime *Phys. Rev.* D **54** 5123 (*Preprint* gr-qc/9604009)
[31] Visser M 1997 Gravitational vacuum polarization: IV. Energy conditions in the Unruh vacuum *Phys. Rev.* D **56** 936 (*Preprint* gr-qc/9703001)